III-3

Chemistry

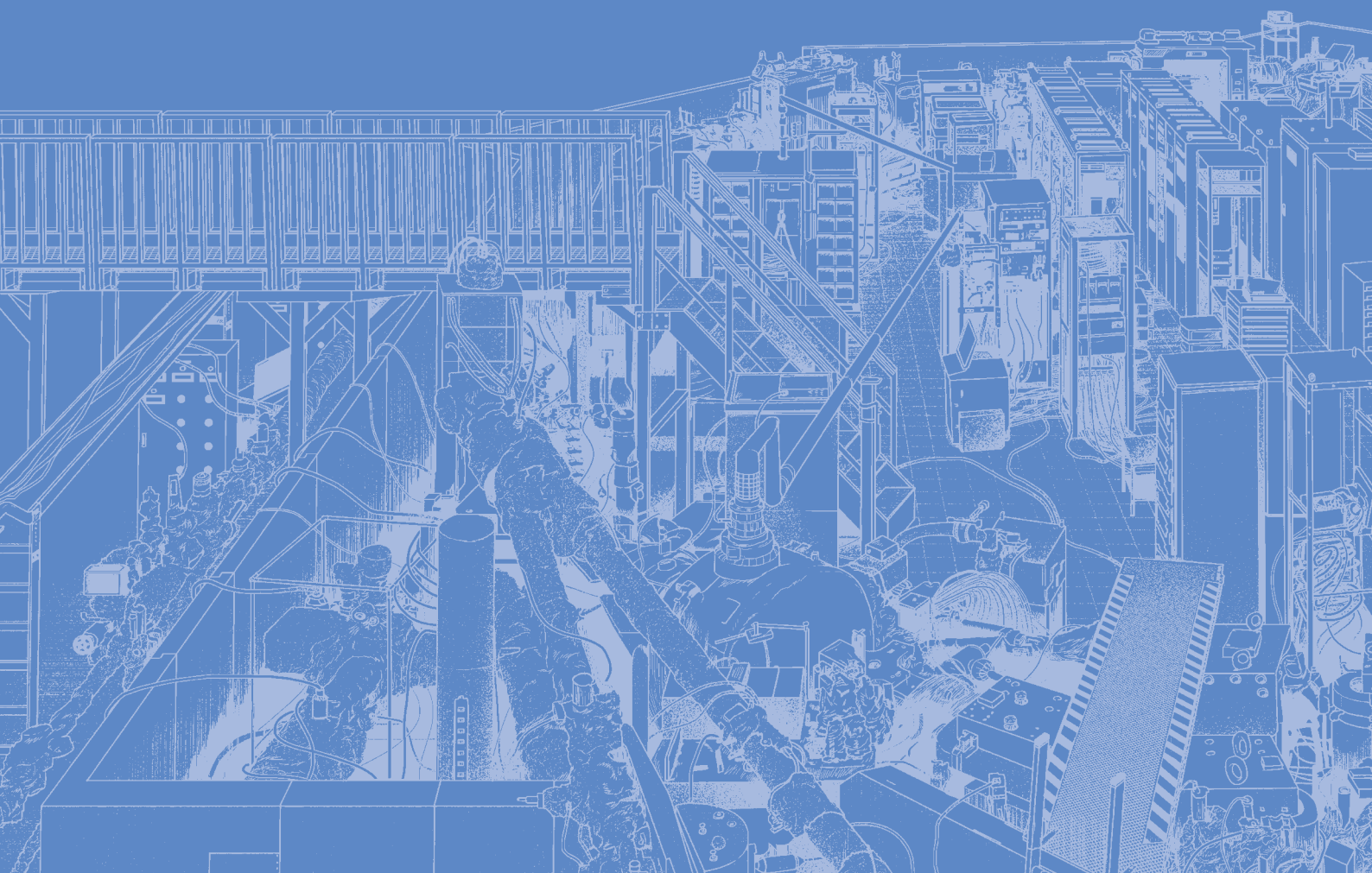

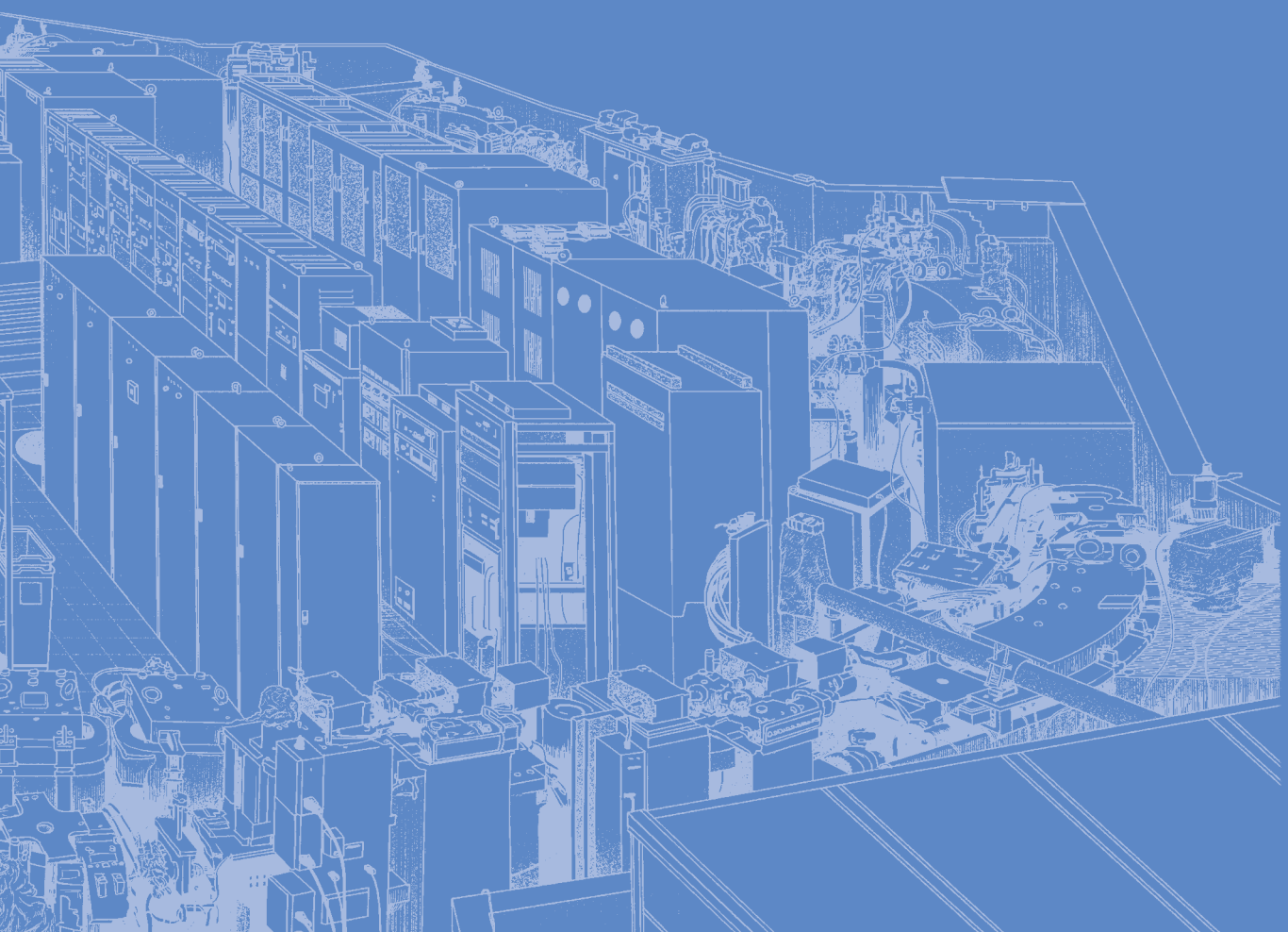

BL1U

Photoionized Plasma Production Experiments in the Synchrotron Light Source UVSOR

M Kobayashi[1], S Yoshimura[1], H Ota[2,3], H Chimura[1], K Shimizu[3], T Kaneyasu[3,4] and M Katoh[3,5]

[1]*National Institute for Fusion Science, Toki city 509-5292, Japan*

[2]*Japan Synchrotron Radiation Research Institute, 1-1-1, Kouto, Sayo-cho, Sayo-gun, Hyogo 679-5198, Japan,*

[3]*UVSOR Synchrotron Facility, Institute for Molecular Science, Okazaki city 444-8585, Japan*

[4]*SAGA Light Source, Tosu city 841-0005, Japan*

[5]*Reserach Institute for Synchrotron Radiation Science, Hiroshima University, Higashi-Hiroshima 739-0046, Japan*

Photoexcitation and photoionization are important processes in space to produce plasmas. The photoinduced processes will also become important in divertor region of nuclear fusion reactors due to both the increase in gas pressure and in the emission from plasmas. In the photoionized plasmas, there is no threshold energy to initiate discharge such as Paschen's law in the electric field application. The cross section of the photoionization decays rapidly with increasing photon energy. The photon energy exceeding the ionization potential is converted to kinetic energy of electrons. Owing to these features, photoionized plasmas are expected to have distinct characteristics from those produced by electric field application, which is usual scheme to produce plasmas in laboratory experiments. In particular, the photoionization rate coefficients become large at several tens eV range for most of atoms and molecules. However, photoionized plasma experiments with systematic scan of photon energy in this range have not been performed so far. Therefore, understanding plasma properties, particularly in terms of plasma as collective phenomena of charged particles, is still very limited. In these contexts, we are developing experimental apparatus that can generate photoionized plasmas by using the synchrotron light source [1], which is capable to change the energy of the beam continuously in a wide range, from X-ray, EUV, VUV, visible, to infra-red ranges.

The VUV/EUV beam was produced in the undulator beam line BL1U in UVSOR. The higher-order light of the undulator beam is cut by gold and an aluminum mirror located on the upstream gas cell, as shown in Fig.1. The cut-off energy is selectable by changing an incident angle of the beam to the mirrors, and it was set to 40eV in the present experiments. The gas cell is connected to the beamline with a multi-step differential exhaust system without a vacuum shielding with a window or film, to avoid flux attenuation caused by the window or film. The photon flux of an order of 10^{15} photons/sec/mm^2 with a beam radius of about 1 mm is obtained at the center of the gas cell. Sample gas was introduced to the gas cell in a range from 1 to 10 Pa, while keeping the high vacuum condition, an order of $10^{-6} \sim 10^{-7}$ Pa, at the upstream chamber connected to the storage ring.

The beam energy was scanned from 16 to 36 eV. The production of photoionized plasmas was detected with emission spectra of the gas and the Langmuir probe measurements. Figure 2 shows a camera image of the Ar plasmas produced by beam energy of 22 eV, where the emission along the beam is clearly observed. The estimated plasma parameters are electron density of order of 10^{13} m^{-3} and electron temperature of about 1 eV at a position 1 mm away from the beam axis. The density decays quickly within 2 mm away from the beam, while temperature is almost constant in space. Analysis of emission spectra to evaluate plasma parameters will be conducted for comparison with the Langmuir probe measurements.

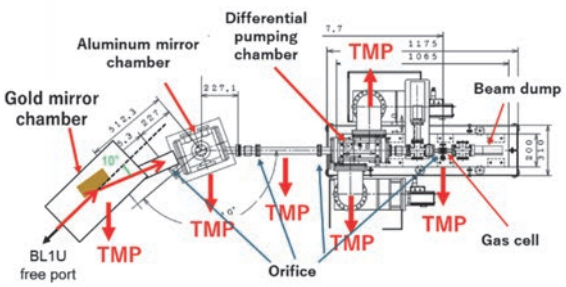

Fig. 1. Schematic of experimental set of photoionized plasma experiments. TMP denotes turbo molecular pump.

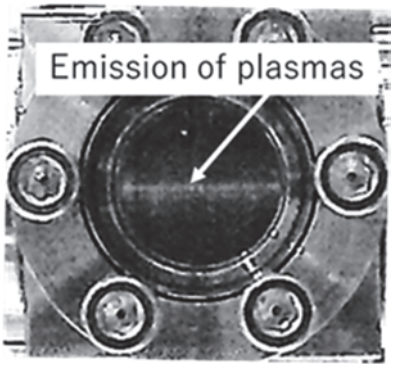

Fig. 2. Visible camera image of photoionized plasmas produced with argon gas of 10 Pa and beam energy of 22 eV. Emission along the beam is clearly observed.

[1] M. Kobayashi *et al.*, Plasma Fusion Res. **19** (2024) 1301038.

BL1U

State-Resolved Molecular Chirality Based on the High-Precision Measurements of Photoelectron Circular Dichroism

H. Kohguchi[1], Y. Hikosaka[2], T Kaneyasu[3], S. Wada[1], K. Shimizu[4], M. Katoh[1,4] and Y-I. Suzuki[5]

[1]*Graduate School of Advanced Science and Engineering, Hiroshima University, Higashi-Hiroshima 739-8526, Japan*

[2]*Institute of Liberal Arts and Sciences, University of Toyama, Toyama 930-0194, Japan*

[3]*SAGA Light Source, Tosu 841-0005, Japan*

[4]*UVSOR Synchrotron Facility, Institute for Molecular Science, Okazaki 444-8585, Japan*

[5]*School of Medical Technology, Health Sciences University of Hokkaido, Tobetsu 061-0293, Japan*

Molecular chirality is generally defined by the molecular structure regarding whether the configuration has a right-handed or left-handed form. Photoelectron circular dichroism (PECD) has been developed as a new approach to examining electronic molecular chirality, which is state-specific and energy-dependent. The BL1U beamline with the undulator is most suited for the PECD study since the circularly polarized light for photoionization is available with the light source in a broad wavelength region. Especially, the BL1U beamline is advantageous for circularly polarized light in the VUV region where PECD is maximized in most chiral molecules [1]. We have investigated the PECD of oxirane with the BL1U beamline and the photoelectron imaging apparatus based on the VMI method.

Oxiranes are typical chiral molecules exhibiting PECD, for which we have conducted the precise measurements of the state- and energy-dependence to compare with our accurate theoretical calculations. The circularly polarized radiation at several wavelengths from 50 nm to 130 nm was used for photoionization. Examples of the observed photoelectron images at various photoionization wavelengths are shown in Fig. 1. The PECD data are difference images between the photoelectron images with the right- and left-circular polarization. The total image intensity was normalized before subtraction. A possible source of inaccuracy occurs in the normalization and background correction of the single polarization image data. The error due to the image data analysis most seriously appears in the highest photoelectron kinetic energy (PKE) region. The photoelectron count rate was suppressed to be lower than 10 kcps by reducing the pulse energy, although the much higher count rate was easily obtained with the BL1U beamline. The number of photoelectrons was limited because our imaging system was too slow to detect correctly more photoelectron spot images on the phosphor screen than 10 kcps. These technical problems could be serious only for the determination of the highly precise PECD parameters. We examined the source of the problems and the solution to improve the accuracy based on the experimental data [2].

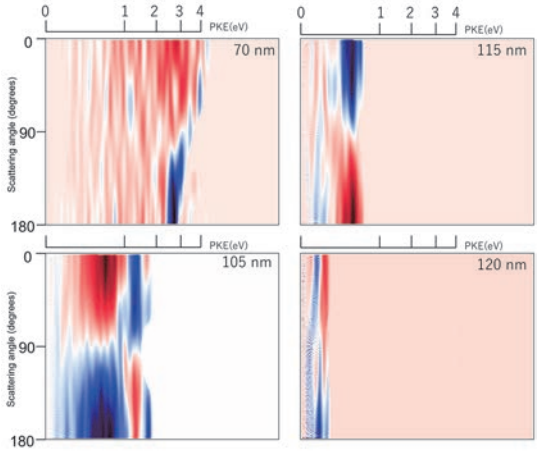

Fig. 1. Photoelectron circular dichroism of methyl oxirane at photoionization wavelengths of 70 nm, 105 nm, 115 nm, and 120 nm. The photoelectron kinetic energy (PKE) is denoted on the upper bar and the scattering angle is indicated on the vertical axis. The partly missing signal region in the largest PKE edge is due to the image data subtraction.

Nevertheless, the state- and energy-dependence of the PECD data are observed (Fig. 1). The PECD was the largest in the low PKE region at the longest photoionization wavelength, which was assigned to the emitted electron from the HOMO and HOMO-1. The sign of PECD (blue/red in Fig. 1) was altered depending on the ionization final states, and the degree of PECD of the particular state varied with the photon energy, therefore PKE. Overall, the PECD decreased with the higher PKE. In the high photon energy (ex. 70 nm in Fig. 1), although the PECD almost disappeared, the highest PKE component exhibited substantially large intensity, indicating a particular state- and energy dependence to reveal the origin of PECD.

[1] H. Kohguchi *et al.*, UVSOR Activity Report **51** (2023) 138.

[2] H. Kohguchi, Y. Hikosaka, T Kaneyasu, S. Wada, and Y-I. Suzuki, UVSOR Activity Report **50** (2022) 136.

BL1U

Inner-Shell Photoelectron Wave Packet Interference by Attosecond Phase Control of XUV Synchrotron Radiation

T. Kaneyasu[1,2], Y. Hikosaka[3], S. Wada[4], H. Ota[5,2], H. Iwayama[2], K. Shimizu[2], M. Fujimoto[6,7] and M. Katoh[8,2,6]

[1]*SAGA Light Source, Tosu 841-0005, Japan*
[2]*Institute for Molecular Science, Okazaki 444-8585, Japan*
[3]*Institute of Liberal Arts and Sciences, University of Toyama, Toyama 930-0194, Japan*
[4]*Graduate School of Advanced Science and Engineering, Hiroshima University, Higashi-Hiroshima 739-8526, Japan*
[5]*Japan Synchrotron Radiation Research Institute, Hyogo 679-5198, Japan*
[6]*Synchrotron Radiation Research Center, Nagoya University, Nagoya 464-8603, Japan*
[7]*Aichi Synchrotron Radiation Center, Seto 480-0965, Japan*
[8]*Research Institute for Synchrotron Radiation Science, Hiroshima University, Higashi-Hiroshima 739-0046, Japan*

The sequential interaction of an atom with a pair of coherent light pulses results in the production of a pair of photoelectron wave packets which interfere with each other during the propagation in a free space. The control and observation of photoelectron wave packet interference has been achieved by using coherent pulse pairs generated by laser sources [1]. Recently, we have shown that the phase coherent double pulses generated by synchrotron light source can be used for controlling the photoelectron wave packet interference in the extreme ultraviolet wavelength [2].

As a next step, we applied this method to the inner-shell ionization of atoms for probing the ultrafast electronic rearrangement processes following the inner-shell ionization of atoms. The experiment was performed by using coherent double pulses generated by a tandem undulator at BL1U. The central photon energy of the pulse was set to approximately 93 eV. The time delay between the pulses was adjusted in femtosecond range with an attosecond resolution. The photoelectron interferogram which comprises of photoelectron spectra measured as a function of time delay, was obtained for helium 1s and xenon 4d photoelectrons.

Figure 1 shows the measured photoelectron interferograms. The interferogram exhibits a periodic modulation due to the interference with a period of approximately 45 as, which corresponds to the photon frequency calculated as $\omega = (E+E_{IP})/\hbar$ where E and E_{IP} are the kinetic energy of the photoelectron and the ionization potential of the atom, respectively. When comparing the two measurements, the contrast of interference quickly decreases as the time delay increases for xenon atoms. This can be explained by the femtosecond Auger decay following the inner-shell ionization. Moreover, the interferogram exhibits intensity modulation with a period of about 2 fs. This effect can be attributed to the evolution of the spin-orbit wave packet produced in the Xe^+ ion, suggesting that this method could be used to explore ultrafast quantum state dynamics with attosecond resolution.

[1] M. Wollenhaupt *et al*., Phys. Rev. Lett. **89** (2002) 173001.
[2] T. Kaneyasu *et al*., Sci. Rep. **13** (2023) 6142.

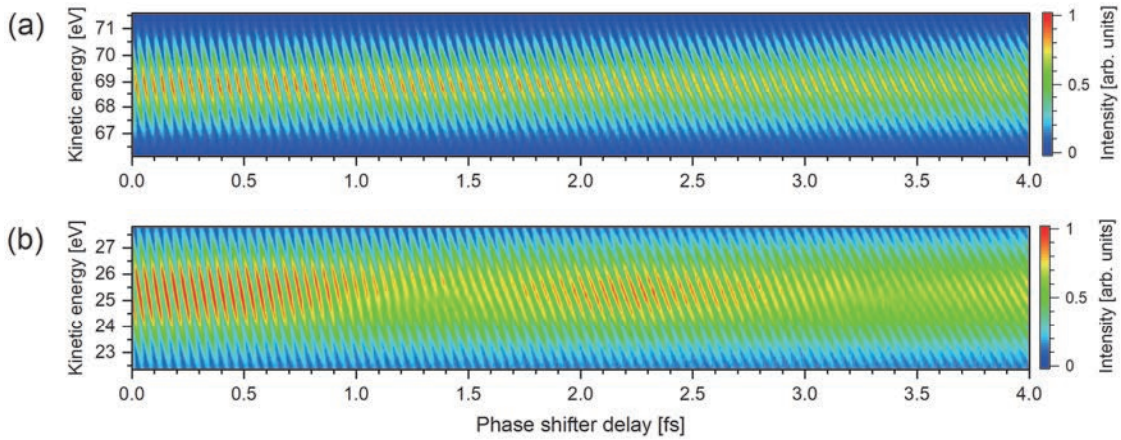

Fig. 1. Photoelectron interferograms measured for (a) helium 1s and for (b) xenon 4d photoelectrons.

BL3U

Oxygen K-Edge Soft X-Ray Absorption Spectroscopy of Pd/CeO_2 Catalyst for DC-Assisted Dry Reforming of Methane

H. Tedzuka[1], N. Matsumoto[1], H. Saito[2], T. Sugimoto[2,3], M. Nagasaka[2,3] and Y. Sekine[1]
[1]*Department of Applied Chemistry, Waseda University, 3-4-1, Okubo, Shinjuku, Tokyo 169-8555, Japan*
[2]*Institute of Molecular Science, Myodaiji, Okazaki 444-8585, Japan*
[3]*Graduate Institute for Advanced Studies, SOKENDAI, Myodaiji,Okazaki 444-8585, Japan*

Chemical utilization of methane (CH_4) and carbon dioxide (CO_2) is of great importance because both are greenhouse gases. Catalytic dry reforming of methane (DRM; $CH_4+CO_2 \rightarrow 2CO+2H_2$) is therefore much attractive reaction in which CH_4 and CO_2 are converted syngas, i.e., the mixture of carbon monoxide (CO) and hydrogen (H_2). In particular, DRM can be a powerful solution of biogas (the mixture of CH_4 and CO_2) utilization [1].

In the conventional DRM induced by thermal catalysis, high reaction temperatures above 973 K are required for activation of CH_4 and CO_2 because both molecules are highly stable. From the thermodynamic point of view, high reaction temperatures are also profitable for achieving high equilibrium conversion. However, under the harsh reaction conditions, catalysts are rapidly deactivated by carbon deposition through CH_4 decomposition ($CH_4 \rightarrow C+2H_2$) and CO disproportionation ($2CO \rightarrow C+CO_2$). Therefore, non-thermal catalytic DRM processes at low temperatures are desirable for suppression of the coke formation and efficient energy utilization.

To promote DRM at low temperatures, we have developed DC-assisted catalysis in which constant DC of the order of a few mA is applied to the catalyst [2]. In this catalytic system, ceria (CeO_2)-supported metal catalysts exhibit high catalytic performance [2]. However, it remains a challenge to elucidate why DRM can be driven at low temperatures, although we reported the key role of surface lattice oxygen species [3]. In this study, to obtain microscopic insight into the reaction mechanism, we performed oxygen *K*-edge soft X-ray absorption spectroscopy (SXAS) of the CeO_2-supoorted palladium (Pd) catalyst.

Pd/CeO_2 was prepared by an impregnation method; firstly, CeO_2 (JRC-CEO-1; Catalysis Society of Japan) and distilled water were added to a flask and were stirred for 2 h, then palladium acetate (Kanto Chemical Co. Inc.) solved in acetone was added into the flask and was further stirred for 2 h. After the suspension was evaporated, the obtained powder was dried at 393 K and calcined at 773 K. For the SXAS measurement, the calcined powder was formed into a pellet.

The SXAS measurement was performed at the BL3U beamline of UVSOR-III synchrotron. After the sample was put on the cell, the chamber was evacuated by a turbomolecular pump. Then, the mixture of CH_4, CO_2 and He, was introduced in the chamber and DRM was induced by applying DC to the sample. SXAS spectra were measured in fluorescence yield mode with a silicon drift detector.

Figure 1 shows the O *K*-edge SXA spectra of the Pd/CeO_2 before and after the reaction. In the spectra before the reaction, two peaks at 529.8 and 532.9 eV were observed. These peaks are attributed to the hybridized O2p-Ce4f state at 529.8 eV and the hybridized O2p-Ce5d(e_g) state at 532.9 eV [4].

Compared with the spectra before the reaction, the two peaks derived from CeO_2 were shifted to the lower energy after the DRM reaction. The shift of the hybridized O2p-Ce5d(e_g) state indicates that a part of Ce^{4+} was reduced to Ce^{3+} during the reaction [5] whereas the shift in the hybridized O2p-Ce4f state suggest the change in the local environment of Ce^{4+}. These results suggest that the redox properties of Ce play a crucial role in the DC-assisted DRM reaction.

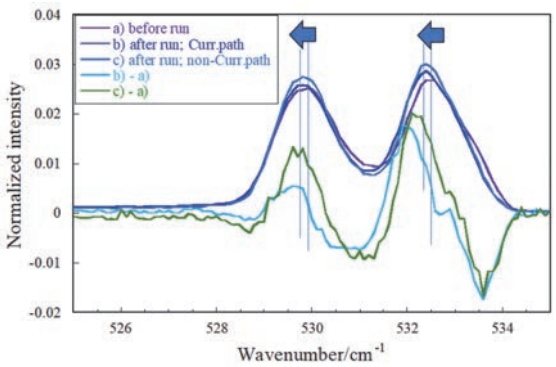

Fig. 1. Oxygen *K*-edge spectra of 1wt%Pd/CeO_2 before and after the DRM reaction. The spectra were measured in fluorescence mode using a silicon drift detector. The DRM reaction was performed by applying DC to the catalyst at $P_{CO2}=P_{CH4}=P_{He}=5$ kPa.

[1] M. Usman *et al.*, Renew. Sustain. Energy Rev. **45** (2015) 710.
[2] A. Motomura *et al.*, RSC Adv. **12** (2022) 28359; A Motomura *et al.*, Chem. Lett. **52** (2023) 259.
[3] N. Nakano *et al.*, RSC Adv. **12** (2022) 9036.
[4] L. Amidani *et al.*, J. Phys. Chem. *C* **127** (2023) 3077.
[5] A.B. Altman *et al.*, Dalton Trans. **45** (2016) 9948.

III-3

BL3U

XAS Measurements for Grahpene Oxide Aqueous Solutions

T. Sasaki[1] and H. Xu[1]
[1]*Department of Complexity Science and Engineering, Graduate School of Frontier Sciences, The University of Tokyo, Kashiwa 277-8561, Japan*

XAS measurements for liquid samples have been enabled at UVSOR BL3U, giving new insights for physicochemical properties of materials [1]. We have achieved O-K edge XAS measurements for cellobiose aqueous solutions and found that XAS signals can be simulated with CP2K and hydrogen bonding with water molecules affect the relative intensity of XAS peaks [2]. In this study Graphene oxide (GO) was chosen as a target molecule. GO is widely used as a catalyst support due to its hydrophilic, acidic, large surface area, and easy modification properties. However, although several structural models have been proposed, none have been conclusively established. We are searching for a suitable structural model for graphene oxide based on quantum chemical calculations, clarifying the dependence of the model on the carbon number, oxygen content, and degree of unsaturation. In particular, we will clarify the functional group structure and carbon defects contained therein and the associated structural features. To verify this, we will perform measurements using soft X-ray absorption spectroscopy and perform simulation calculations of the spectra to experimentally verify the structural model.

XAS measurements for liquid samples were conducted at UVSOR BL3U using facilities developed by Nagasaka et al. [1]. The liquid sample cell with Si3N4 membranes was adopted, where the thickness of the liquid layer was controlled by the He gas pressure around the cell. GO was prepared by the modified Hummers method [3] and aqueous solution was prepared by sonication of 2 hours.

Figure 1 shows C-K XAS spectrum for GO (14 mg) in 10 ml water at room temperature. Three peaks at 285, 287 and 291 eV were observed. O-K XAS measurement was also achieved but due to the dominant contribution by water molecules it was difficult to assign peaks originated from GO (not shown).

We are also conducting computational study for obtaining typical structural formula of GO. In order to clarify the structure of graphene oxide, we performed a structure search using l-ADDF calculations using GRRM, sorted the resulting equilibrium structures (EQs) in order of energy, and enumerated the partial features within the structure for each EQ as structural features, thereby summarizing the energetically stable EQs and their structural features. Multiple l-ADDF calculations with different calculation conditions were conducted, and the trends was clarified as to the results of the structure search (calculation time, number of EQs obtained, number of structural features obtained, and energy width of the EQs obtained) when changing LADD, Nlowest, and calculation level. We also compared previously proposed structures and found the modified structure which exhibits the stabilized total energy with a modified partial structure as shown in Fig. 2. XAS simulation calculation using the obtained GO formula is undertaken to assign the peaks in the experimental result.

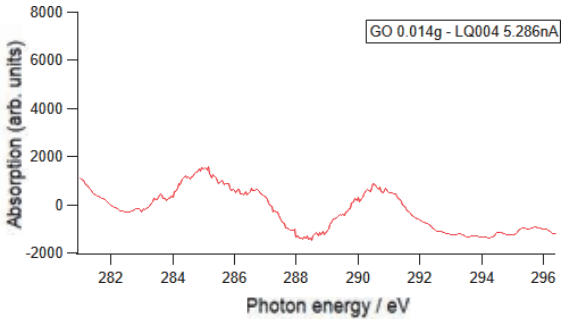

Fig. 1. C-K XAS spectrum for GO (14 mg) in 10 ml water at room temperature.

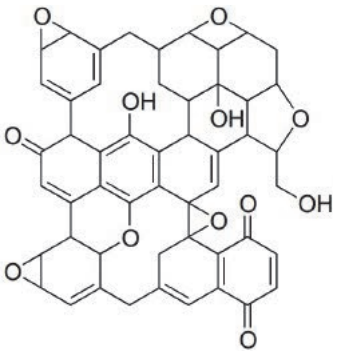

Fig. 2. One of the GO models obtained by GRRM calculation.

[1] M. Nagasaka *et al.*, J. Electrosc. Relat. Phenom. **200** (2015) 293.
[2] D. Akazawa *et al.*, J. Chem. Phys. **156** (2022) 044202.
[3] V.B. Saptal *et al.*, Chem. Sus. Chem. **9** (2016) 644.

BL3U

Salt-Specific Effect on the Solubility and Aggregation of 1-butanol in Water

Y. Yao[1], M. Nagasaka[2,3] and K. Mochizuki[1]
[1]*Department of Chemistry, Zhejiang University, Hangzhou 310028, RP China*
[2]*Institute for Molecular Science, Okazaki 444-8585, Japan*
[3]*Graduate Institute for Advanced Studies, SOKENDAI, Okazaki 444-8585, Japan*

The Hofmeister series has continued to a topic of interest across a variety of fields [1], and the Hofmeister anion series is typically represented by $CO_3^{2-} > SO_4^{2-} > S_2O_3^{2-} > H_2PO_4^- > F^- > Cl^- > Br^- > NO_3^- > I^- > ClO_4^- > SCN^-$. The solubility and aggregation of solute molecules in water has been influenced with the addition of these Hofmeister anions. In this study, the salt-specific effect on the degree of aggregation of 1-butanol molecules in aqueous solutions were studied using C K-edge X-ray absorption spectroscopy (XAS) [2].

The C K-edge XAS experiments were performed at BL3U using the transmitted-type liquid cell, whose details were described previously [3, 4]. The liquid cell was at an ambient pressure in helium gas, where a liquid layer was sandwiched between two Si_3N_4 membranes with a thickness of 100 nm. The thickness of the liquid layer was precisely controlled by adjusting the helium pressure for obtaining appropriate absorbance of soft X-rays. XAS spectra were obtained using the Lambert-Beer law, $\ln(I_0/I)$, where I and I_0 are the transmission signals of aqueous butanol solutions including salts and the solutions without 1-butanol, respectively.

Figure 1 shows C K-edge XAS spectra of 0.2 M aqueous 1-butanol solutions including different salts, where 1 M $NaClO_4$, 1 M NaCl, and 1 M Na_2SO_4 are dissolved. The temperatures of aqueous solutions were kept at 25 °C. The XAS spectra consists of five broad peaks, which were assigned using the inner-shell calculations: The lowest peak is assigned to the transition of the CH_3 C1s electrons to the 3s-type Rydberg orbitals. The second peak is assigned to the transitions of the CH_2 C1s electrons in the center part of the butyl group to the 3s-type Rydberg orbitals. The third peak is assigned to the transitions of the CH_3 C1s electrons to the 3p-type Rydberg orbitals. The fourth peak is assigned to the transitions of the CH_2 C 1s electrons in the center part of the butyl group to the 3p-type Rydberg orbitals. The fifth peak is assigned to the transitions of the CH_2 C1s electrons connected to the hydroxyl groups to the 3s-type Rydberg orbitals.

The peak intensity at 288.5 eV in the XAS spectrum of 0.2 M aqueous 1-butanol solution is higher than that in the spectrum of neat 1-butanol liquid. It is because 1-butanol molecules are remarkably isolated in the dilute aqueous solution. This tendency is same as the C K-edge XAS spectra of aqueous methanol and ethanol solutions [5, 6]. It means that the aggregations of 1-butanol molecules in aqueous solutions would be evaluated from the peak intensities at 288.5 eV.

In the C K-edge XAS spectra of 0.2 M aqueous 1-butanol solutions shown in Fig. 1, the peak intensities at 288.5 eV are decreased with the order of $NaClO_4$, NaCl, and Na_2SO_4 from those with no salt condition. It means that the aggregations of 1-butanol molecules by adding salts are increased with the order of $NaClO_4$, NaCl, and Na_2SO_4. It means that the aggregations of 1-butanol molecules follow the Hofmeister anion series. These results provide molecular insights into how ions affect solute solubility and solute-solute aggregations for other hydrophobic molecules. The C K-edge XAS measurements are useful for evaluating the aggregations of hydrophobic molecules in aqueous solutions.

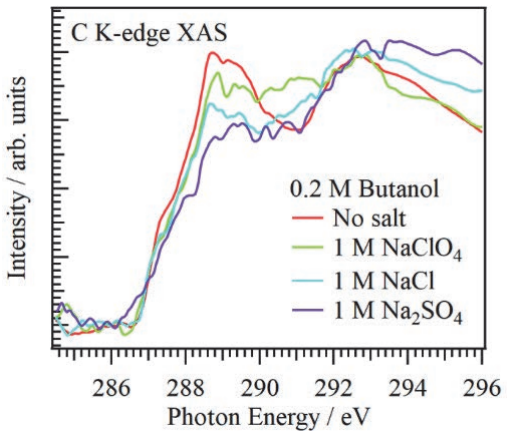

Fig. 1. C K-edge XAS spectra of 0.2 M aqueous 1-butanol solutions including different salts (1 M $NaClO_4$, 1 M NaCl, and 1 M Na_2SO_4).

[1] F. Hofmeister, Arch. Exp. Pathol. Pharmakologie **24** (1888) 247.
[2] Y. Yao *et al*., Physica A **647** (2024) 129917.
[3] M. Nagasaka *et al*., Anal. Sci. **36** (2020) 95.
[4] M. Nagasaka and N. Kosugi, Chem. Lett. **50** (2021) 956.
[5] M. Nagasaka *et al*., J. Phys. Chem. B **118** (2014) 4388.
[6] M. Nagasaka *et al*., J. Phys. Chem. B **126** (2022) 4948.

BL3U

Structure Analysis of Organic Thin-Film Solar Cells Using Resonant Soft X-ray Scattering Technique

H. Iwayama[1] and A. Sugishima[2]
[1]*UVSOR Synchrotron Facility, Institute for Molecular Science, Okazaki 444-8585, Japan*
[2]*Analysis Technology Center, Fujifilm Corporation, Minamiashigara 250-0193, Japan*

Resonant soft X-ray scattering is an innovative technique for analyzing chemical-specific structures in material science. Conventional small-angle X-ray scattering (SAXS) has been widely used to analyze nanostructures within materials. However, when analyzing polymer composites, SAXS faces significant challenges due to the lack of contrast between polymers composed mainly of light elements. This makes it difficult to determine how these polymers mix and interact. For instance, in organic thin-film solar cells, efficient charge transfer is achieved when two molecules form a bulk heterojunction structure. However, this structure is challenging to measure using conventional SAXS.

Resonant soft X-ray scattering (RSoXS) enhances scattering from specific molecules by utilizing their resonant energy differences. This technique takes advantage of the slight differences in resonant X-ray energies between two molecules to clarify their structures and arrangements. This allows for detailed analysis of the internal structures of polymer composites. In this work, we show an example application of RSoXS in the analysis of organic thin-film solar cells.

Our sample is an organic thin film composed of [6,6]-Phenyl-C61-butyric Acid Methyl Ester (PCBM) and Poly(3-hexylthiophene-2,5-diyl) (P3HT) spin-coated on a 100 nm thick Si3N4 membrane, and has a bulk heterojunction structure separated at the nanoscale as shown in Fig. 1. The thickness of this film is about 200 nm.

The experiment was performed at UVSOR BL3U. The soft X-ray energy was 260 eV for non-resonance and 284 eV and 286 eV for resonance, respectively. The camera length was 100 mm, and the scattered light was observed with a soft X-ray camera (Andor BN940P).

Figure 2 shows the scattering profile at the photon energy of 260, 284, and 298 eV. The horizontal axis is the scattering vector q [nm^{-1}], and the vertical axis is the scattering intensity. No strong scattering peak was observed in the non-resonance case of 260 eV. This means that there is no difference in the complex dielectric constant of the two molecules, so there is no contrast in the scattering process. On the other hand, at 284 eV, close to the resonance energy of PCBM, a strong peak was observed at q=0.2 nm^{-1}. This indicates that PCBM has a spatial scale of about 30 nm. On the other hand, at 298 eV, where scatterings from P3HT are enhanced, a peak was also observed at q=0.1 nm^{-1}. This means that P3HT has a spatial scale of about 60 nm.

In our work, it has been shown that the structure of each polymer can be analyzed by using resonant soft X-ray scattering. We will continue to conduct detailed analysis.

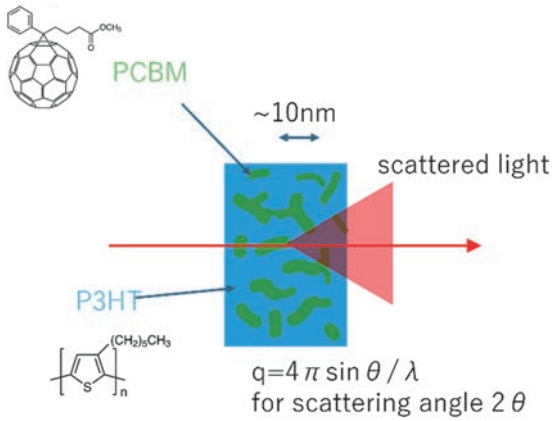

Fig. 1. Schematic view of the organic thin film, where bulk heterojunction of PCBM and P3HT is formed.

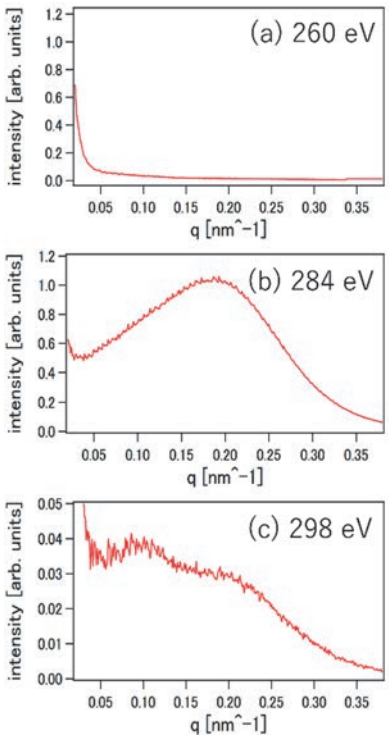

Fig. 2. Scattering profiles for the organic thin film at the photon energies of (a) 260 eV, (b) 284 eV and (c) 298 eV.

BL3U

Observation of O K-Edge X-Ray Absorption Spectrum of μ-Oxo-Bridged Iron Phthalocyanine Dimer

Y. Yamada [1,2] and M. Nagasaka[3]

[1]*Department of Chemistry, Graduate School of Science, Nagoya University, Furo-cho, Chikusa-ku, Nagoya 464-8602, Japan*

[2]*Research Center for Materials Science, Nagoya University, Furo-cho, Chikusa-ku, Nagoya 464-8602, Japan*

[3]*Institute for Molecular Science, Myodaiji, Okazaki 444-8585, Japan*

Coordination of oxygen atoms to the iron porphyrinoids has long been attracted interests of chemists since interactions of oxygen atoms with iron center of iron porphyrin are quite important in various biological processes such as oxygenation, oxygen carrying, and so on. It is well-known that iron(II) porphyrinoids including iron porphyrin and iron phthalocyanine tend to form μ-oxo-bridged dimers as described in Fig. 1 under air [1]. These μ-oxo-bridged dimers of iron porphyrinoids can act as an oxygenation catalyst for various organic chemicals under photoirradiation in the presence of O_2.

To the best of our knowledge, soft X-ray XAS studies of μ-oxo-bridged iron porphyrinoid dimers have not been reported yet, although there are some reports on hard X-ray XAS studies. Therefore, the purpose of this work is to investigate μ-oxo-bridged iron phthalocyanine dimer by soft X-ray XAS. We prepared a μ-oxo-bridged iron phthaloycyanine dimer having 8 peripheral *tert*-butyl units **1** and a monomeric iron(III) phthalocyanine chloride having 4 peripheral *tert*-butyl units **2**. The use of soft X-ray XAS is advantageous because direct and selective observation of both oxygen and iron atoms in an μ-oxo-bridged dimer become possible since the soft-X-ray region include both of the K-edge of oxygen and L-edge of iron.

O K-edge XAS measurements of **1** and **2** in solution were performed by using a beamline equipped with a transmission-type liquid flow cell in BL3U of UVSOR [2]. The spectra were obtained based on the Lambert-Beer law, $\ln(I_0/I)$, where I_0 is the transmission signals of benzonitrile and I is those of **1** or **2**.

Fig. 2 shows a comparison of the O K-edge XAS spectra obtained for **1** and **2** in benzonitrile (30 mM). The blue spectrum represents that of **2** having no oxygen-containing moieties, where small amount of silicon oxide on Si_3N_4 membrane and H_2O in benzonitrile were observed. It is considered that the μ-oxygen of **1** should show double bond character due to the interaction of p-orbitals of the μ-oxygen atom with the d-orbitals of the iron atom of two iron porphyrins. It is known that, generally in the O K-edge XAS spectra, the peaks of oxygen having double bond character tend to appear at lower energy than 534 eV, whereas the peaks of oxygen having single bond character appears at higher energy than 535 eV [3]. By comparing the spectra of **1** and **2**, we considered that the peak at 527 eV and/or 532–534 eV could be assigned to those of μ-oxygen of **1**. In order to identify the peaks of μ-oxygen of **1**, we are going to measure the soft X-ray XAS of the solids of **1** and **2**. In addition, DFT calculations of XAS of **1** and **2** are also underway.

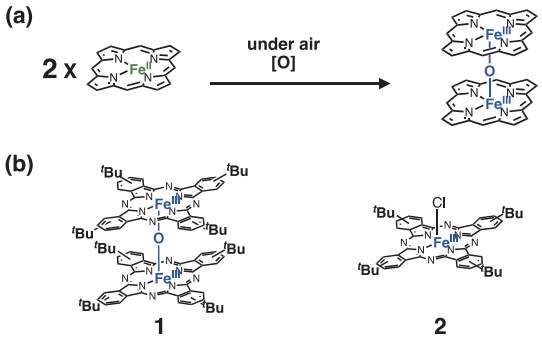

Fig. 1. Generation of μ-oxo-bridged iron porphyrin dimer from iron porphyrin.

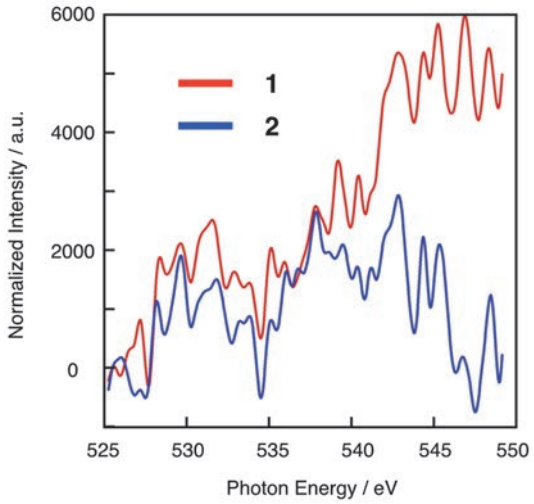

Fig. 2. Comparison of O K-edge XAS spectra of **1** and **2** in benzonitrile (30 mM) at 25 °C.

[1] S. P. Rath *et al.*, Coord. Chem. Rev. **337** (2017) 112.
[2] M. Nagasaka and N, Kosugi, Chem. Lett. **50** (2021) 956.
[3] M. Nagasaka *et al.*, Phys. Chem. Chem. Phys. **26** (2024) 13634.

BL3U

Soft X-ray Absorption Study of a Titanium-Oxide Photocatalyst Suspended in Water

Yi Hao Chew[1], N. Ichikuni[2], T. Yoshida[3] and H. Onishi[1,4]
[1]*Graduate School of Science, Kobe University, Kobe 657-8501, Japan*
[2]*Graduate School of Engineering, Chiba University, Chiba 263-8522, Japan*
[3]*Graduate School of Engineering, Nagoya University, Nagoya 464-8603, Japan*
[4]*Division of Advanced Molecular Science, Institute for Molecular Science, Okazaki 444-8585, Japan*

Material conversion on semiconductor photocatalysts is intensively studied worldwide. Downhill reactions, in which the Gibbs free energy decreases during the conversion of reactants to products, have been successfully integrated into our society [1]. Artificial photosynthesis, a category of uphill reactions involving the oxidation of water, is being developed for societal implementation in the near future [2]. In addition, fundamental studies are being conducted to uncover new scientific discoveries related to light-driven, efficient materials conversion.

In collaboration with Prof. Masanari Nagasaka of UVSOR, we apply soft X-ray absorption to the *in-situ* characterization of semiconductor photocatalysts suspended in water. An anatase TiO_2 photocatalyst (JRC-TIO-19 provided by Catalysis Society of Japan), was suspended in water. The suspended solution was adjusted with NaOH to pH 13. The pH adjustment was critical to suspend 100 nm TiO_2 particles long enough to pass through a liquid cell.

The liquid cell was mounted in BL3U. Oxygen K-edge and titanium L-edge absorption spectra were observed with a transmission setup [3] in the presence and absence of ultraviolet (UV) light for band-gap excitation. Soft X-rays transmitted through the suspended solution were detected with a silicon photodiode. The photodiode was capped with a 150 nm thick aluminum film (LUXEL, TF110) to minimize the contribution of stray UV light to the detector response (Fig. 1). The capping device is deposited at UVSOR. Users are encouraged to use the device when operating the photodiode under UV or visible light irradiation.

Figure 2 shows a Ti L-edge spectrum observed in the presence of UV light provided by a Hg–Xe lamp (200 W). In the Ti L-edge, electron transition from Ti2s and 2p to 3d orbitals of TiO_2 particles appears at 455–470 eV [4]. The Ti3p orbitals are hybridized with O2s and 2p orbitals to form the conduction band in TiO_2. The hybridized orbitals are split into t_{2g} and e_g levels according to the ligand field in TiO_6 octahedra.

The soft X-ray absorption of solutions has been successfully studied. Here, transmission measurement was achieved with a suspension. The extension to an *operando* study of the suspension under UV irradiation is possible.

This study was supported by JSPS KAKENHI (grant number 22H00344).

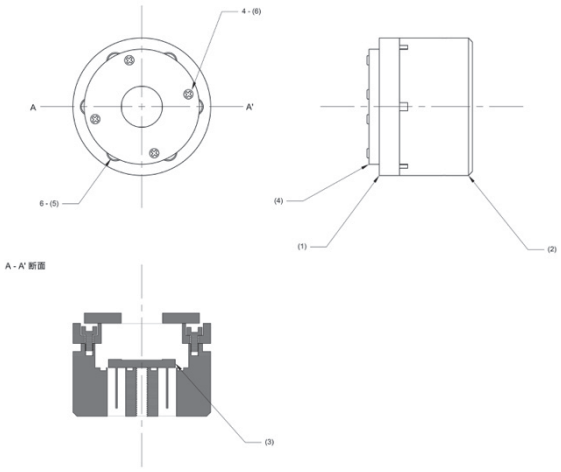

Fig. 1. A devise capping the photodiode with the aluminum filter for transmission detection of soft X-ray absorption spectrum under UV-light irradiation.

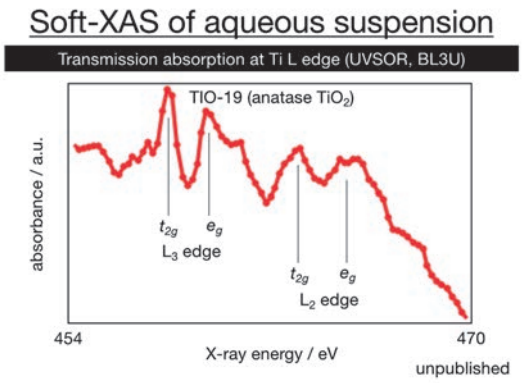

Fig. 2. Soft X-ray absorption of anatase TiO_2 photocatalyst particles (JRC-TIO-19) suspended in water at pH 13. Titanium L-edge spectrum was observed under UV light irradiation.

[1] A. Fujishima *et al.*, J. Photochem. Photobio. C **1** (2000) 1.
[2] H. Onishi, ChemSusChem **12** (2019) 1825.
[3] T. Petit *et al.*, J. Phys. Chem. Lett. **6** (2015) 2909.
[4] S. C. Ray *et al.*, J. Phys. Chem. C **126** (2022) 8947.

BL3U

Direct Observation of Solvation of Redox Species by Soft X-ray Spectroscopy toward Development of High Performance Thermo-Electrochemical Cells

H. Yoshikawa[1], K. Wakamatsu[1], Z. Hongyao[2], T. Yamada[2] and M. Nagasaka[3]

[1]*Program of Materials Science, School of Engineering, Kwansei Gakuin University, Sanda, Hyogo 669-1330, Japan*

[2]*Division of Chemistry, Graduate School of Science, The University of Tokyo, Bunkyo-ku, Tokyo 113-0033, Japan*

[3]*UVSOR Synchrotron Facility, Institute for Molecular Science, Okazaki, Aichi 444-8585, Japan*

In the utilization of primary energy, approximately 50–60 % is discarded as unused waste, with around 70 % of this being low-grade waste heat. The recovery and reuse of low-grade waste heat using thermoelectric devices, which convert thermal energy into electrical energy, present an effective solution to the energy problem. Among various thermoelectric devices, thermochemical cells (TECs) utilizing liquid electrolytes have recently gained attention due to their high thermoelectric conversion efficiency [1]. The efficiency of thermoelectric conversion is evaluated by the dimensionless figure of merit as following:

$$ZT = \frac{S_e^2 \sigma T}{\kappa} \quad (1)$$

where S_e is Seebeck coefficient, σ is electrical conductivity, T is temperature, and κ is thermal conductivity. To enhance thermoelectric conversion efficiency, the material must exhibit a high S_e, excellent σ, and low κ. However, achieving all these properties simultaneously in a single material remains a significant challenge. To establish an ideal reaction mechanism and molecular design guidelines, it is crucial to observe the reaction field. However, X-ray structural analysis of fluids, particularly liquids, is challenging and remains largely unexplored. In this study, we identified the redox pair quinone/hydroquinone in sodium chloride solution under flow conditions.

The functional group discrimination of quinone/hydroquinone in aqueous NaCl solution was investigated by measuring carbon (C) *K*-edge X-ray absorption spectroscopy (XAS) spectra. The XAS measuremnt was conducted at BL3U of UVSOR equipped with a transmission liquid flow cell [2]. The energy range was set to 280–300 eV, with grating widths of 129 μm/61 μm (S_0/S_1). A 100 mM NaCl solution served as the standard (baseline) sample, to which 10 mM quinone and hydroquinone were added, respectively. The XAS spectra were analyzed based on Lambert-Beer's law as following:

$$\mu t = \ln \frac{I_0}{I_1} \quad (2)$$

where μ is absorption coefficients, t is sample thickness, and I_0 and I_1 represent the incident and transmitted light intensities, respectively. The XAS spectra of 10 mM quinone/hydroquinone in aqueous NaCl solution were applied baseline correction using those of the 100 mM NaCl solution.

The peaks observed at 285.9 eV and 293.0 eV correspond to C1s–π* of C=C and C1s–σ* of C=C resonances, respectively (Fig. 1), indicating their origin from the six-membered rings of quinone and hydroquinone. The intense peak at 288.4 eV corresponds to a C1s–π* of C=O resonance (Fig. 1), suggesting its association with the quinone functional group. These findings confirm the detection of quinone and hydroquinone signatures in the spectrum, demonstrating that their functional groups can be observed in the fluid phase.

Future studies will use electrochemical measurements and XAS analysis at BL3U to further clarify the redox mechanism in TECs with quinone-based systems. Solvation by redox species and solvents is crucial for TEC performance. To explore solvation effects, including hydrogen bonding, *operando* soft X-ray XAS will be conducted on solutions with dissolved redox species. We will examine how solvation influences redox behavior under different solvent compositions, acidity levels, and electrolyte concentrations. These insights will aid in optimizing thermochemical energy conversion systems.

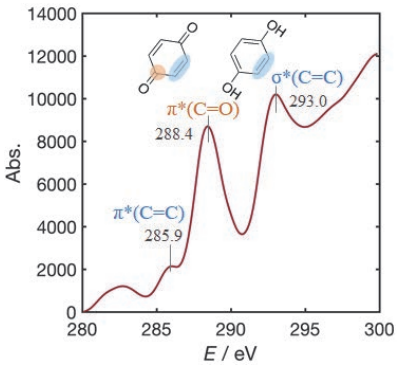

Fig. 1. C *K*-edge XAS spectra of 10 mM quinone/hydroquinone in 100 mM NaCl solution.

[1] H. Zhou *et al*., Angew. Chem. Int. Ed. **62** (2023) e202213449.

[2] M. Nagasaka *et al*., Chem. Lett. **50** (2021) 956.

III-3

BL3U

The Electronic States of 1-Methylimidazole in the Acetic Acid/1- Methylimidazole Mixture

Y. Horikawa[1], Y. Shiro[1] and M. Nagasaka[2]

[1]*Graduate School of Sciences and Technology for Innovation, Yamaguchi University, Yamaguchi 753-8512, Japan*

[2]*Institute for Molecular Science, Okazaki 444-8585, Japan*

We have observed the electronic structure of acetic acid and 1-methylimidazole (1-MI) molecules in their solution by soft X-ray spectroscopy to investigate the cause of the change in electrical conductivity of 1- MI/ acetic acid mixtures [1, 2]. The electrical conductivity of the solutions changes drastically when the mixing ratio is changed, with maxima at mole fractions of acetic acid (χ_{AcO}) of 0.65 and 0.85. The results of previous analyses showed that the ionic content of acetic acid and 1-MI was maximum around $\chi_{AcO} = 0.70$, while the ionic content decreased at concentrations of $\chi_{AcO} = 0.85$. The reason why the electrical conductivity reaches a maximum value at the high acetic acid concentration, despite the decreasing amount of ions, is thought to be due not only to the diffusion of the ionic molecules (acetic acid ions and 1-MI ions) themselves, but also to the proton hopping between the acetic acid monomers and 1-MI or through acetic acid chain clusters. However, the previous measurements have only been made to analyze the molecular species in the mixed solution under steady-state conditions. Since an electric field is applied to the solution when electrical conduction occurs, the application of an electric field generates acetate ions that do not exist under steady-state conditions, and the possibility of an increase in electrical conductivity due to the diffusion of these ions was considered. In this experiment, the electronic state of acetic acid molecules in the mixed solution was observed in an electrochemical cell during the application of an electric field to confirm whether new ions were generated.

Soft X-ray absorption spectroscopy measurements at the O K-edge were performed using a transmission electrochemical cell for the solution. Fig. 1 and 2 show the absorption spectra of acetic acid at $\chi_{AcO} = 0.70$ and 0.85 with and without the application of an electric field. As 1-MI dose not contain any oxygen atoms, the absorption spectra at the O K-edge only reflect information about the acetic acid molecules. Previous studies have shown that absorption peaks originating from the $O_{C=O}$ $1s \rightarrow \pi^*_{OCO}$ and O_{OH} $1s \rightarrow \pi^*_{OCO}$ transitions appear at around 532.6 eV and 535 eV for molecules containing the COOH group. When the carboxy group ionises to COO^-, the two oxygen atoms become chemically equivalent, the positions of the two absorption peaks coincide and the second peak no longer appears [1]. In other words, as the acetate neutral molecules in solution become acetate ions, or as more acetate ions come close to the electrode surface, the intensity of the second peak is expected to decrease as the overall spectral shape. Figure 1 shows that the intensity of the second peak was 0.50 relative to the first peak without the application of an electric field, while the intensity of the second peak was 0.36 when an electric field of 0.7 V was applied, indicating a clear decrease in the intensity of the second peak. However, no effect of the electric field application was observed for the solution with mole fraction $\chi_{AcO} = 0.85$, and it was experimentally confirmed that the application of the electric field caused the formation of acetate ions and that the increase in conductivity due to the increase in ion content was unlikely to have occurred. This result supports the idea that proton hopping is the cause of the increase in conductivity in the solution with mole fraction $\chi_{AcO} \sim 0.85$.

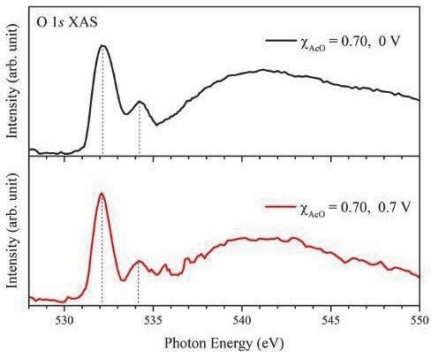

Fig. 1. O K-edge X-ray absorption spectra of acetic acid in the solution of $\chi_{AcO} = 0.70$ with and without the application of an electric field.

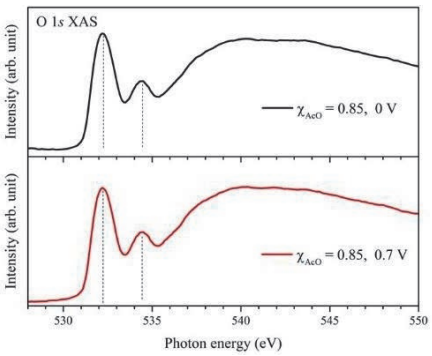

Fig. 2. O K-edge X-ray absorption spectra of acetic acid in the solution of $\chi_{AcO} = 0.85$.

[1] N. Yoshimura *et al*., J. Phys. Chem. B **123** (2019) 1332.

[2] Y. Horikawa, M. Okazaki and M. Nagasaka, UVSOR Activity Report **51** (2023) 129.

BL3B

Valence Fragmentation Dynamics of a Promising Low Global Warming Etching Gas CF_3CHCF_2

Tran T. Nguyen[1], T. Hayashi[1], H. Iwayama[2] and K. Ishikawa[1]
[1]*Nagoya University, Furo, Chikusa, Nagoya 464-8601, Japan*
[2]*UVSOR Synchrotron Facility, Institute for Molecular Science, Okazaki 444-8585, Japan*

The semiconductor industry faces significant challenges in etching high-aspect-ratio (HAR) structures for fabrication of 3D flash memory. Traditional reactive ion etching (RIE) processes struggle with issues on aspect-ratio-dependent etching and require precise control to maintain high-quality profiles [1]. Hydrofluorocarbons (HFCs) and perfluorocarbons (PFCs) gases are widely used in the HAR etching processes; despite their impact on global warming. To address these environmental concerns, the industry is exploring alternative gas chemistries and process techniques, including low-GWP fluorocarbons [2, 3].

In this study, we have investigated dissociation of C_3HF_5 by the PEPICO (Photo Electron Photo Ion CO incidence) technique using synchrotron radiation [4]. Identifying key dissociative fragments provided valuable insights for optimization of the etching results and minimization of their environmental impact.

The PEPICO experiments were conducted at the UVSOR facility in Japan, utilizing a 2.5 m off-plane Eagle-type monochromator to generate tunable vacuum ultraviolet (VUV) light in the energy range of 10-26 eV. C_3HF_5 gas was introduced into a high-vacuum chamber and irradiated with the VUV light. A time-of-flight mass spectrometer was employed to detect the resulting fragment ions. By analyzing the ion yield curves as a function of photon energy, appearance energies were determined, providing valuable insights into the dissociation pathways and energetics of C_3HF_5 molecules.

The dissociative photoionization of C_3HF_5 was systematically characterized across 10–26 eV using PEPICO spectroscopy. At 20 eV, the mass spectrum revealed dominant fragment ions such as $C_3HF_4^+$ and $C_3F_4^+$, alongside significant contributions from CF_3^+ and $C_2F_3^+$. The parent ion $C_3HF_5^+$ persisted at this energy, while weaker signals for smaller fragments (e.g., $C_3F_3^+$, $C_2F_2^+$) suggested secondary dissociation pathways. Figure 1 shows a breakdown diagram constructed from the ion yield curves. The breakdown diagram illustrated a photon-energy-dependent evolution in fragmentation: below 14 eV, the parent ion dominated (~80% abundance), with minor $C_3F_5^+$ (~20%) from H loss. Above 14 eV, a sharp transition occurred, with $C_3HF_4^+$ (F loss) and $C_3F_4^+$ (HF loss) emerging as primary products, collectively contributing ~54% of the ion yield by 15.5 eV. Notably, CF_3^+ became increasingly prominent above 15.2 eV, reaching ~25% abundance at 19–26 eV. Appearance energies (AEs), derived from ion yield thresholds, confirmed sequential fragmentation: the parent ion $C_3HF_5^+$ originated at 10.6 ± 0.06 eV, followed by $C_3F_5^+$ (10.7 ± 0.03 eV). $C_3HF_4^+$ exhibited dual pathways (13.7 ± 0.02 eV and 14.2 ± 0.04 eV), attributed to distinct C–F bond cleavages in CF_3 and CF_2 groups, while $C_3F_4^+$ showed similar dual thresholds (13.5 ± 0.02 eV and 14.5 ± 0.03 eV). Secondary fragments (e.g., CF^+) emerged above 17.9 eV but contributed minimally (<3%), underscoring the dominance of primary dissociation channels.

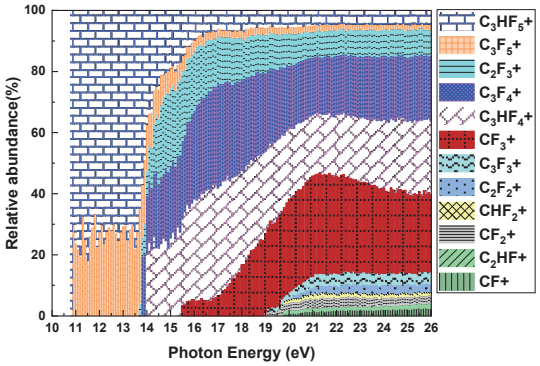

Fig. 1. Relative abundance curves of the fragment ions produced from the photoionization of C_3HF_5.

C_3HF_5 fragmentation balances fluorine-rich (CF_3^+, $C_3F_4^+$) and hydrogen-containing ($C_3HF_4^+$) species, critical for SiO_2/SiN etching. Fluorine radicals enhance SiO_2 etching, while hydrogen promotes polymer deposition for selectivity. Below 14 eV, minimal fragmentation favors parent ions; higher energies (>15 eV) optimize reactive fragment yields. The AE data align with plasma conditions (1–5 eV electron energies), suggesting C_3HF_5 efficiency in generating key etching species at low thresholds.

C_3HF_5 low-energy fragmentation pathways, characterized by PEPICO, validate its suitability as an eco-friendly etching gas. Optimizing photon energy controls reactive species, advancing high-aspect-ratio etching in semiconductor manufacturing. This study provides a framework for designing next-generation low-GWP etching gases.

[1] S. N. Hsiao *et al.*, Appl. Surf. Sci. **542** (2021) 148439.
[2] T. N. Tran *et al.*, Appl. Surf. Sci. **684** (2025) 161815.
[3] C. Abe *et al.*, Jpn. J. Appl. Phys. **63** (2024) 06SP10.
[4] T. N. Tran, *et al.*, Sci. Rep. **15** (2025) 9507.

BL4B

Dissociation Following Double Auger Decay of Xenon Difluoride Molecules

Y. Hikosaka[1]
[1]*Institute of Liberal Arts and Sciences, University of Toyama, Toyama 930-0194, Japan*

Molecular inner-shell photoionization is usually followed by Auger decay, where occasionally two Auger electrons are emitted, resulting in the formation of triply-charged molecular ions. These ions are energetically unstable due to Coulomb repulsion among the three positive charges and typically fragment immediately after their formation. In this study, we employed multielectron-ion coincidence spectroscopy with a magnetic bottle electron spectrometer equipped with ion detection [1,2] to explore the dissociation of triply-charged states in xenon difluoride (XeF_2) [3], a molecule characterized by weak bonding between the central rare-gas atom and fluorine ligands.

The double Auger decay processes of the XeF_2 4d core-hole state can be isolated through electron triple coincidence which includes a 4d photoelectron. Figure 1 (top) displays the energy sum of the two other electrons detected in coincidence with a $4d_{3/2}$ photoelectron as a function of the XeF_2^{3+} binding energy, determined by the relationship: (XeF_2^{3+} binding energy) = ($4d_{3/2}^{-1}$ binding energy) − (sum of two Auger electrons' energy). The ratio of double to single Auger decay in the $4d_{3/2}^{-1}$ state is determined to be 33% ± 5%, considering electron detection efficiency. The XeF_2^{3+} spectrum generally shows a gradual rise from around 60 eV without distinct peaks. The triple ionization threshold is about 4 eV lower than that of atomic Xe. The observed triple ionization threshold for double Auger decay can be less than the vertical triple ionization energy. This discrepancy arises because the double Auger decay involves sequential processes that pass through the intermediate XeF_2^{2+} states, which lie below the vertical triple ionization energy. The second Auger steps originating from these XeF_2^{2+} states occur outside the Franck–Condon region of neutral ground state XeF_2.

Four ion species, Xe^{2+}, Xe^+, F^+, and XeF^{2+}, were detected in coincidence with the triple electrons including a $4d_{3/2}$ photoelectron. The dissociation pathways potentially forming these four ions are $Xe^{2+} + F^+ + F$, $Xe^+ + 2F^+$, and $XeF^{2+} + F^+$. To elucidate the contributions from these pathways, XeF_2^{3+} spectra filtered with these four ion species were obtained from fourfold coincidences between the three electrons and an ion. Figure 1 illustrates the coincidence spectra. The spectra corresponding to Xe^{2+}, Xe^+, and XeF^{2+} delineate the contributions from the dissociation pathways of $Xe^{2+} + F^+ + F$, $Xe^+ + 2F^+$, and $XeF^{2+} + F^+$, respectively. The spectrum coincident with F^+ includes contributions from all the dissociation pathways.

Dissociation to $XeF^{2+} + F^+$ occurs just above the triple ionization threshold and peaks around 60 eV. Dissociation to $Xe^+ + 2F^+$ begins around 62 eV and reaches its maximum near 68 eV. The onset of dissociation to $Xe^{2+} + F^+ + F$ is around 65 eV, with yield rapidly increasing as binding energy increases.

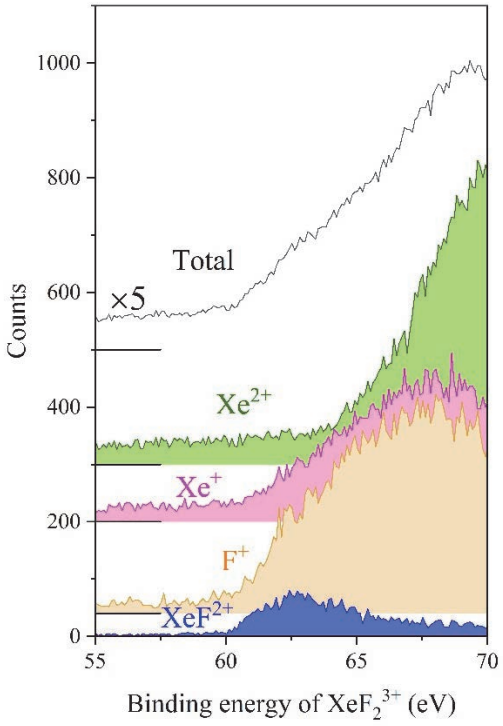

Fig. 1. Spectra of XeF_2^{3+} states selected by coincidence with fragment ions and the overall XeF_2^{3+} spectrum resulting from the $4d_{3/2}$ double Auger decay.

[1] Y. Hikosaka and E. Shigemasa, Int. J. Mass Spectrom. **439** (2019) 13.
[2] Y, Hikosaka, J. Electron Spectrosc. Relat. Phenom. **255** (2022) 147158.
[3] Y. Hikosaka, J. Chem. Phys. **160** (2024) 024304.

BL4B

X-ray Absorption Spectroscopy in Ferroelectric Nematic Liquid Crystals

F. Araoka[1], Y. Takanishi[2] and H. Iwayama[3]
[1]*RIKEN Center for Emergent Matter Science, Hirosawa 2-1, Wako, Saitama 351-0198, Japan*
[2]*Department of Physics, Kyoto Prefectural University of Medicine,1-5, Shimogamohangi-cho, Sakyo, Kyoto 606- 0823, Japan*
[3]*UVSOR Synchrotron Facility, Institute for Molecular Science, Okazaki 444-8585, Japan*

Ferroelectric nematics (NF) are a new group of polar fluid liquid crystals (LCs), wherein liquid-like fluidity and ferroelectricity co-exist. Such polar ordering was first predicted by the well-known physicist, Max Born, in the early 20th century. However, it had not been realized for a long time until its coincident discoveries in 2017 by two independent groups [1,2]. There are many fascinating physical properties of NF such as huge apparent permittivity values, large spontaneous polarization, strong nonlinear optical effects, and so on. Because of both scientific curiosity and vast potential for applications, it has attracted broad attention in the field of liquid crystal sciences.

Recently, we reported cybotactic cluster formation stabilizing the NF phase in diastereomeric DIO mixtures [3]. In this case, anisotropy of the smectic clusters, estimated from small/wide angle X-ray analysis, clearly shows growth of clusters as temperature decreases. This suggests a possibility that the side-by-side interaction may be an important role in stabilizing the polar ordering of the NF phase. Motivated by this, we have tackled resonant X-ray scattering to resolve polar distribution at the nanoscopic scale. However, due to strong absorption at the carbon K-edge, yet it is too difficult to detect a clear scattering pattern. Thus, we need to seek the possibility to use other resonant conditions in other elements, such as fluorine, or oxygen, which also takes a part of the molecular structure of the NF molecule.

In this study, we performed X-ray absorption spectroscopy for the NF liquid crystal, DIO-C3 (Fig. 1, left). The carbon, fluorine, and oxygen K-edge absorption spectra were taken by scanning the photon energy of the soft X-ray irradiated on the sample sandwiched between two silicon nitride (SiN) membrane films (Fig. 1). The sample film was heated by a hot stage which equips input/output window to allow the X-ray beam to pass through. The transmitted X-ray was detected by a photodiode instead of a cooled CCD used in the scattering experiment, and the generated photocurrent was recorded by a signal counter.

Plotted in Fig. 2 are typical carbon K-edge absorption spectra taken using the soft X-ray beam at BL3U. The spectra show two signature peak regions; one appearing in the lowest photon energy region (285~6 eV) is corresponding to the π-electrons in the molecule, the other in the higher energy region (above~286.5eV) to the α-electrons. Interestingly, the latter shows notable peak shift at the phase transition temperature between the nematic, antiferroelectric meso- and NF phases, while the former shows only scarce change either in the peak position or shape. This means, the head-to-tail dipolar interaction, which affects the longitudinal α-orbitals, is stronger than the effect of the side-by-side attraction contributed from the π-π interaction, in the present system. Thus, this is different from our expectation, described in the above introduction part. Based on this result, we further conducted K-edge absorption measurements for fluorene and oxygen by using the soft X-ray available at BL4B. The result will be discussed with a theoretically computed spectrum obtained with a density functional theory (DFT). Further calculation and analysis are currently on-going.

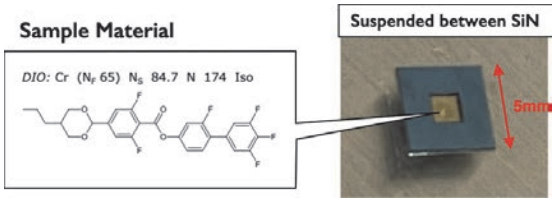

Fig. 1. Chemical structure of the NF molecule, DIO-C3 (Left), introduced between two SiN membrain films (Right).

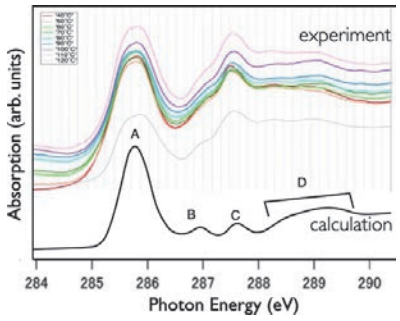

Fig. 2. Typical temperature-dependent absorption spectrum in the NF material, DIO-C3. The region A is corresponding to the π-orbital, and B, C and D are to the α-orbitals of alkyls and dioxanes.

[1] H. Nishikawa *et al.*, Adv. Mater. **29** (2017) 1702354.
[2] R. Mandle *et al.*, Chem. Eur. J. **23** (2017) 14554.
[3] H. Nishikawa *et al.*, Commun. Mater. **3** (2022) 89.

III-3

BL4B

Fragmentation Processes of 2-Iodothiophone in Doubly Charged States Studied by Multielectron-Ion Coincidence Spectroscopy

M. Fushitani[1], Y. Hikosaka[2], Y. Kimura[1] and A. Hishikawa[1,3]

[1]*Graduate School of Science, Nagoya University, Nagoya 464-8602, Japan*

[2]*Institute of Liberal Arts and Sciences, University of Toyama, Toyama 930-0194, Japan*

[3]*Research Center for Materials Science, Nagoya University, Nagoya 464-8602, Japan*

Breaking chemical bonds in a cyclic structure is an important step for ring-opening reactions. Among others, 2-iodothiophene (2-C_4H_3SI) is one of the prototype heterocyclic compounds which have been used to clarify the elementary processes in photoinduced ring-opening. Site-selective probing using ultrashort laser pulses in the extreme ultraviolet (EUV) and X-ray region is a promising method to directly capture details of the reaction [1, 2]. Such inner-shell probing often leads to the formation of highly charged states followed by ultrafast dissociation into different channels. Since the fragmentation pathways could be dependent on the initial geometry, it offers a unique approach to understand photoinduced processes in neutral states, including the ring-opening. Herein, we carried out multielectron-ion coincidence spectroscopy of I 4d inner-shell photoionization of 2-C_4H_3SI in the ground state to study the fragmentation processes after the core-hole decay.

Synchrotron radiation at 105 eV (single bunch mode) was used to ionize isolated 2-C_4H_3SI molecules and the produced electrons and ions were detected in coincidence by using a magnetic bottle type electron spectrometer with an ion-collecting electrodes [3,4].

The measured ion time-of-flight mass spectrum identifies formations of C_n (n = 1-4) hydrocarbons with a specific number of H atoms. Figure 1(a) shows I $4d_{5/2}$ Auger electron spectrum obtained in coincidence with I $4d_{5/2}$ photoelectrons and the parent 2-$C_4H_3SI^{2+}$ ions in the ground state while those with pairs of I^+ and the counterpart fragment ions are shown in Figs.1(b)-(i). All the Auger signals for the ion pairs appear in the lower energy region than the Auger peak at 33.1 eV of the parent 2-$C_4H_3SI^{2+}$, showing that these fragmentations take place mainly in electronically excited states in the doubly charged states. The Auger signals associated with the fragment ions can be classified into the 0-20 eV (Region I) and 20-32 eV (Region II) energy regions. It is found in Fig. 1(c) that $C_3H_3^+$ ions are selectively produced with I^+ ions in Region II while in Region I the fragment ions become C_3H^+ species instead of $C_3H_3^+$. On the other hand, C_4 and C_2 hydrocarbons in Figs. 1(b) and (d), appear as C_4H^+ and $C_2H_2^+$ ions, both of which are identified in Region I only. This suggests that a three-body fragmentation, 2-$C_4H_3SI^{2+} \rightarrow C_3H_3^+ + I^+ +$ CS, is a main channel to break the ring structure in Region II.

Auger signals for the fragment ions containing the S atom in Figs. 1(e)-(i), it turns out that $C_3H_3S^+$, C_2HS^+, CHS^+, and S^+ ions with a fixed number of H atoms are dominant products as the I^+ counterpart while for $C_4H_nS^+$ (n = 0-3) ions the number of the H atom depends on the Auger electron energies. It is noted that the Auger peak at 30.4 eV for the (I^+, $C_4H_3S^+$) ion in Fig. 1(e) exhibits much narrower spectral width compared to the other Auger peaks. This indicates that the $C_4H_3S^+$ moiety could keep its cyclic structure after the C-I bond fission, 2-$C_4H_3SI^{2+} \rightarrow C_4H_3S^+ + I^+$.

The present study reveals which electronic energy region of 2-$C_4H_3SI^{2+}$ preferentially produces specific fragment pair of ions with the characteristic numbers of C and H atoms, providing crucial information on the ring-opening processes.

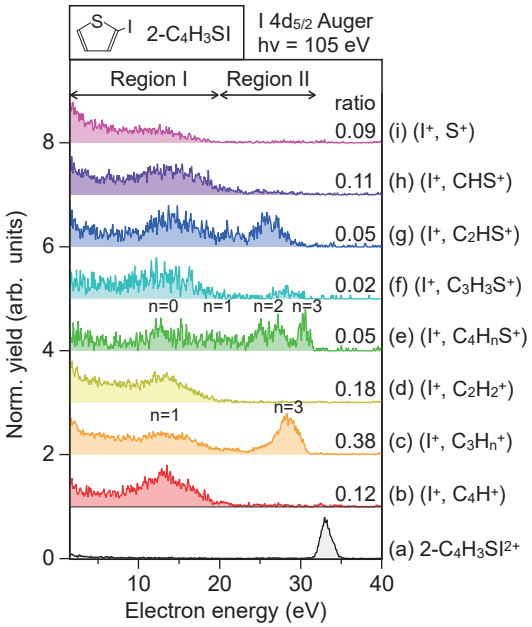

Fig. 1. Auger electron spectra of 2-iodothiophone by I $4d_{5/2}$ inner-shell photoionization at 105 eV, detected in coincidence with (a) 2-$C_4H_3SI^{2+}$, (b) (I^+, C_4H^+), (c) (I^+, $C_3H_n^+$(n = 1,3)), (d) (I^+, $C_2H_2^+$), (e) (I^+, $C_4H_nS^+$(n = 0-3)), (f) (I^+, $C_3H_3S^+$), (g) (I^+, C_2HS^+), (h) (I^+, CHS^+), and (i) (I^+, S^+) ions. The values for traces (b)-(i) represent the relative yield among these ion pairs.

[1] B. W. Toulson *et al.*, J. Chem. Phys. **159** (2023) 034304.

[2] W. O. Razmus *et al.*, Phys. Chem. Chem. Phys. **26** (2024) 12725.

[3] Y. Hikosaka, J. Electron Spectrosc. Rel. Phenom. **255** (2022) 147158.

[4] M. Fushitani *et al.*, J. Chem. Phys. **160** (2024) 174307.

BL5B

Development of the Fast Camera System for High-Precision Photoelectron Imaging

H. Kohguchi[1], Y. Hikosaka[2], T Kaneyasu[3], S. Wada[1], K. Shimizu[4], M. Katoh[1,4] and Y-I. Suzuki[5]

[1]*Graduate School of Advanced Science and Engineering, Hiroshima University, Higashi-Hiroshima 739-8526, Japan*

[2]*Institute of Liberal Arts and Sciences, University of Toyama, Toyama 930-0194, Japan*

[3]*SAGA Light Source, Tosu 841-0005, Japan*

[4]*UVSOR Synchrotron Facility, Institute for Molecular Science, Okazaki 444-8585, Japan*

[5]*School of Medical Technology, Health Sciences University of Hokkaido, Tobetsu 061-0293, Japan*

Recent development of photoelectron circular dichroism (PECD) studies significantly relies on photoelectron VMI (Velocity Map Imaging) measurements as well as circularly polarized radiation generated with undular light sources, which is especially advantageous for one-photon ionization in the vicinity of the molecular photoionization threshold region. On the other hand, multi-photon ionization based on laser-based photoionization has also been subject to the PECD research. Molecular electronic chirality can be further understood in comparison with the PECD data of one-photon and multi-photon ionization.[1, 2]

We have so far used the camera system of the VMI apparatus common for laser and synchrotron light sources, although the synchrotron measurements and laser-based measurements were executed in UVSOR and the Hiroshima University laboratory, respectively. Besides the wavelength regions, the critical difference of the UVSOR beam line and the pulsed laser system regarding our PECD study lies in the repetition rate and the photoelectron count rate. The pseudo-continuous radiation provided by the UVSOR beam line can generate photoelectrons with more than 100 kcps (counts per second) under our experimental conditions. The pulsed laser system runs in a 10 Hz repetition rate, where a single laser shot provides less than 100 photoelectrons corresponding to the 10 cps. The photoelectron count rate should be reduced to a rate so low that the light spots due to a single photoelectron arrival at the detector do not overlap each other, otherwise, the accurate photoelectron distributions are not obtained. The higher count rate, ensuring the better signal statistics, is especially critical in PECD measurements, where the difference of independently measured image data is analyzed. In place of the conventional frame-transfer type camera (1000 x 1000 pixels, 33 frames/s rate), which was matched with the low repetition pulsed laser, we introduced an event-driven type camera, whose nominal signal transfer rate is sufficiently fast to fully capture the signals provided by the UVSOR beam line.

The performance of the event-driven camera was examined with the BL5B beam line. The camera equipped with the VMI apparatus was linked with the local Ethernet LAN to store the event data. The sensitivity, temporal response, and transfer rate were methyl oxirane at 120 nm (Fig. 1). Although the photoelectron spot images were overlapped in a frame-type camera display (Fig. 1(a)-(c)), the stored event data were confirmed to be isolated from each other by the fast time resolution of 1 μs (Fig. 1(d)). We developed a program code to recover the image data from the event data. The results indicated the good linearity of the image intensity up to the photoelectron count rate of 500 kcps, which is nearly the upper limit of the detector damage.

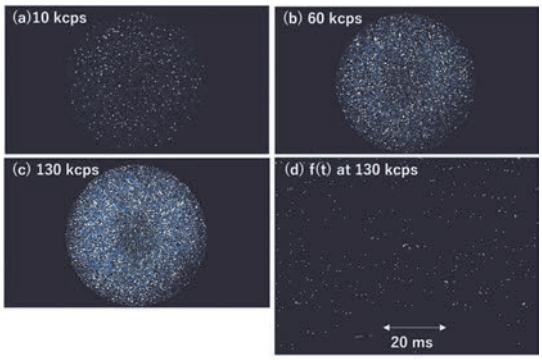

Fig. 1. Photoelectron image data measured with the event-driven camera equipped with the synchrotron radiation light source. The light spots due to photoelectron hitting on the imaging detector (1280 x 720 pixel size) accumulated in 33 camera frames are shown at a photoelectron count rate of (a) 10 kcps, (b) 60 kcps, and (c) 130 kcps. A time profile of the event-camera output in a particular pixel column of (c) is shown in (d).

[1] H. Kohguchi *et al.*, UVSOR Activity Report **50** (2023) 138.
[2] H. Kohguchi *et al.*, UVSOR Activity Report **50** (2022) 136.

BL3B, 5B, 7B

Delayed Fragmentation of Ethanol Molecules Induced by Photoionization

T. Nakao[1], T. Kaneyasu[2,3], H. Iwayama[3], T. Yanagawaya[4] and T. Majima[1]
[1]*Department of Nuclear Engineering, Kyoto University, Kyoto 615-8540, Japan*
[2]*SAGA Light Source, Tosu 841-0005, Japan*
[3]*Institute for Molecular Science, Okazaki 444-8585, Japan*
[4]*Faculty of Engineering, Kyoto University, Kyoto 606-8501, Japan*

Characterizing the intermediate states of ionized and excited molecules before dissociation is a key to understanding the fragmentation mechanism. Valuable insights into the intermediate states can be obtained through an analysis of the delayed fragmentation processes. We investigated the delayed fragmentation from various singly charged intermediate ions by coincidence measurement of product ions and neutral fragments using time-of-flight (TOF) mass spectrometry [1]. We have observed delayed fragmentation from nucleobase (adenine, guanine, cytosine, thymine, and uracil) and alcohol (ethanol, 1-propanol, and 2-propanol) molecules induced by MeV-energy fast ion collisions so far. The results indicated that large degrees of freedom are essential to the delayed fragmentation from singly charged intermediate ions. However, due to the complexity of fast-ion-induced processes, the characteristics of intermediate ions are not fully understood. In this study, we carried out photoionization experiments in the vacuum ultraviolet (VUV) region.

The experiments were performed at the bending magnet beamlines BL3B, BL5B, and BL7B of the UVSOR III facility. The main measurement was performed at BL7B after the test experiments at BL3B and BL5B. Monochromatic VUV light in the range of 13.0–23.0 eV photon energy was delivered to the experimental apparatus equipped with a TOF mass spectrometer. Effusive molecular beam of ethanol was used as the target. Fragments were detected with a microchannel plate (MCP) detector and recorded in event-by-event mode by a multichannel scaler.

Figure 1 shows TOF correlation spectra of the two fragments measured at a photon energy of 18.0 eV. Delayed fragmentation processes from singly charged intermediate ions are clearly visible as long diagonal tails extend from spots. Note that in this experiment neutral fragments are detectable in the delayed fragmentation, although the detection efficiency of them is relatively low due to the insufficient impact energy to be detected by the MCP. This is because they are generated during the extraction from the ionization region to the drift tube.

The delayed fragmentation channels were identified by comparing the experimental results and the calculated curves shown on the right side of Fig.1. The numbers in the figure correspond to the following channels: (1) $C_2H_5O^+ \rightarrow CHO^+ + CH_4$, (2) $C_2H_5O^+ \rightarrow C_2H_3^+ + H_2O$, (3) $C_2H_5O^+ \rightarrow H_3O^+ + C_2H_2$, and (4) $C_2H_3O^+ \rightarrow CH_3^+ + CO$. These pathways are the same as the MeV-energy fast ion collisions. The delayed fragmentation events at the tails in Fig. 1 indicate that the intermediate ions remain undissociated for submicroseconds.

The photon energy dependence of each delayed fragmentation channel was investigated, except for channel 2 because of the low statistics. Channel 1 and channel 3 show a similar energy dependence: the tail appears rapidly at about 14 eV. For channel 3, the tail appears gradually at about 17 eV. Since the vertical ionization potential of ethanol is about 10.6 eV [2], the results indicate that these delayed fragmentation processes can be induced with an internal energy of a few eV. These threshold energies are consistent with the preliminary results of the quantum chemical calculations we performed.

The photon energy dependence of the decay curve of the intermediate ion $C_2H_5O^+$ on channel 3 was also obtained by analyzing TOF spectra. The decay curve shows a $1/t$ dependence above 15 eV. This result indicates that the internal energy transferred to vibrational excitation is the key to delayed fragmentation.

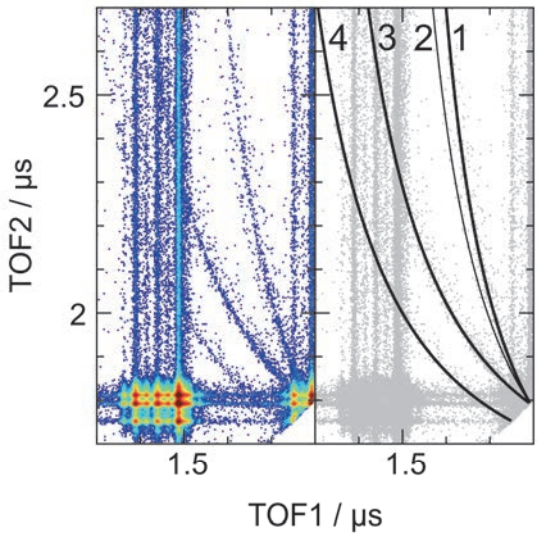

Fig. 1. TOF correlation spectra at 18.0 eV. Four delayed fragmentation channels were determined by comparing the experimental results (left) and the calculated curves (right). The numbers correspond to each dissociation channel.

[1] T. Nakao *et al.*, J. Chem. Phys. **161** (2024) 054302.
[2] P. Linusson *et al.*, Phys. Rev. A **80** (2009) 032516.

BL7B

High-Resolution Photoelectron Spectroscopy of Functional Compounds with High Melting Points

H. Kohguchi[1], Y. Hikosaka[2], T Kaneyasu[3], S. Wada[1], K. Shimizu[4], M. Katoh[1,4] and Y-I. Suzuki[5]

[1]*Graduate School of Advanced Science and Engineering, Hiroshima University, Higashi-Hiroshima 739-8526, Japan*

[2]*Institute of Liberal Arts and Sciences, University of Toyama, Toyama 930-0194, Japan*

[3]*SAGA Light Source, Tosu 841-0005, Japan*

[4]*UVSOR Synchrotron Facility, Institute for Molecular Science, Okazaki 444-8585, Japan*

[5]*School of Medical Technology, Health Sciences University of Hokkaido, Tobetsu 061-0293, Japan*

Photoelectron circular dichroism (PECD) has been investigated with a photoelectron imaging apparatus based on the velocity-mapping imaging (VMI) methodology. The targets of the PECD study have been mostly limited to gaseous or volatile samples since photoelectron imaging relies on electron detection under high vacuum conditions. Chiral compounds in solid form are not subjects of the PECD study, although much more chiral species with novel chirality are stable than gaseous and volatile liquid samples. We have developed the VMI photoelectron imaging apparatus for PECD measurement, providing high-quality PECD data for gaseous chiral molecules [1]. Application of the VMI apparatus to solid chiral samples requires the generation of the molecular beam by heating solid samples. The molecular beam intensity was found to be much weaker than that of the gaseous beams in our previous studies [2]. Thus, efficient photoelectron data collection is a key to PECD measurements of solid chiral species as well as intense beam sources with a heat nozzle.

A photoelectron count rate for gaseous samples is typically several hundred kcps under our experimental conditions. Although the count rate can be increased by more than 1000 kcps, our previous image detection system could only acquire less than 100 kcps photoelectrons because of the slow frame transfer rate (33 frames/s) of the camera system. In the present measurement with the BL7B beamline, we have adopted an event-driven camera to a spot image of a photoelectron arrival on the phosphor screen, whose nominal response time is potentially one microsecond.

We examined the sensitivity and operative limitation of the event-driven camera for the actual PECD measurement conditions but the Ar sample was used for evaluation. The results of photoelectron imaging of Ar at 76 nm photoionization are shown in Fig. 1. The photoelectron image obtained with the conventional frame camera exhibited noticeable background noise outside of photoelectron scattering distribution (Fig. 1a). The background, which originated from the analog recording, was found to be critical for in our previous PECD study because difference image data between right- and left circularly polarization ionization is heavily affected by preceding signal normalization. It is noted that the electron background, which originates from the photoionization of the imperfectly evacuated samples in the vacuum chamber subtraction, is not problematic in image subtraction. The image data captured with the event-driven camera at various count rates (Fig. 1b-1d) indicated that no photoelectron arrival position on the phosphor screen was lost up to the count rate of 180 kcps. The photoelectron spectra and the angular distributions with 5 kcps, 40 kcps, and 180 kcps are identical other than the signal statistics. Application of the event-driven camera to the photoelectron imaging with synchrotron radiation, especially to the image subtraction, is thus confirmed.

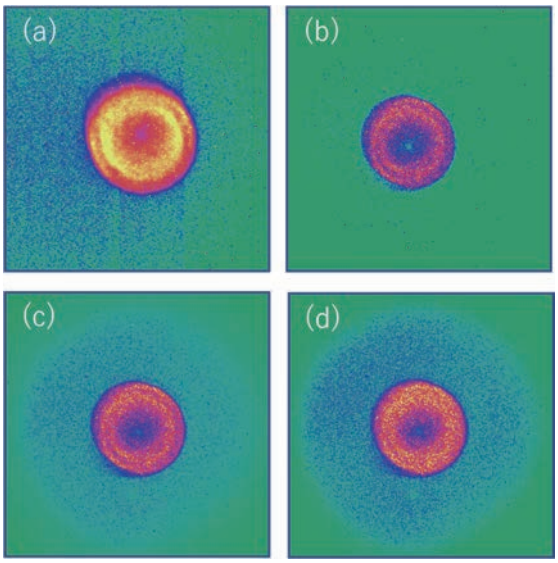

Fig. 1. Photoelectron scattering images of Ar at 76 nm photoionization with (a) the frame-camera (conventional) and (b)–(d) the event-driven camera. The electron count rate is (b) 5 kcps, (c) 40 kcps and (d) 180 kcps. The outside of the double-ring image is especially emphasized to display the background level.

[1] H. Kohguchi *et al.*, UVSOR Activity Report **50** (2023) 138.

III-3

UVSOR User 11

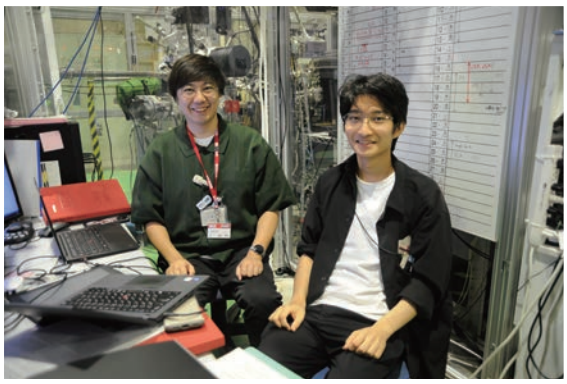

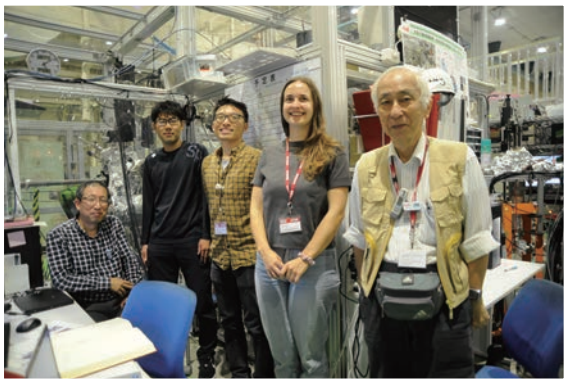

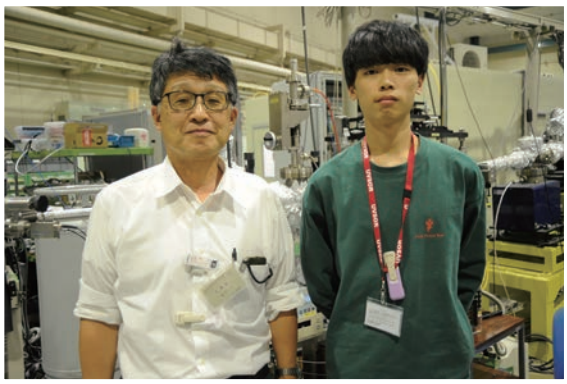

UVSOR User 12